Desalination and Water Treatment
www.deswater.com

doi: 10.1080/19443994.2016.1166459

57 (2016) 27279–27293
December

Taylor & Francis
Taylor & Francis Group

Simultaneous removal of phosphate and ammonium using salt–thermal-activated and lanthanum-doped zeolite: fixed-bed column and mechanism study

Yinhai He[a,b], Hai Lin[a,*], Yingbo Dong[a,b], Quanli Liu[a,b], Liang Wang[a,b]

[a]*School of Civil and Environmental Engineering, University of Science and Technology Beijing, Beijing 100083, China, Tel. +86 18811349855; email: hyh19881226@163.com (Y. He), Tel. +86 13801283734; Fax: +86 010 62332526; email: linhai@ces.ustb.edu.cn (H. Lin), Tel. +86 13810931697; email: ybdong@ustb.edu.cn (Y. Dong), Tel. +86 18810640357; email: lqlquanli@gmail.com (Q. Liu), Tel. +86 18810919421; email: Lking198905@163.com (L. Wang)*
[b]*Beijing Key Laboratory on Resource-Oriented Treatment of Industrial Pollutants, Beijing 100083, China*

Received 27 October 2015; Accepted 12 March 2016

ABSTRACT

Assessment of breakthrough performance of NaCl–Thermal–$LaCl_3$ synthetic modified zeolite continuous flow fixed-bed column on the simultaneous removal of phosphate and ammonium from simulated municipal wastewater was conducted. Variable parameters, including solution pH, bed depth, effluent flow rate, and input concentration, were examined for this study. The results indicated that the adsorption capacity increased with the increase in bed depth and input concentration and decrease of effluent flow rate for both phosphate and ammonium. Thomas and Yoon–Nelson models were found to give the better fitness to experiment data of the whole breakthrough curves, whereas Adams–Bohart model could only predict the initial part of the breakthrough using linear regression analysis. The bed depth service time model of breakthrough data showed that the time for the movement of the mass transfer zone increased with the increase in bed height and flow rate and decrease in initial concentration. Best fixed-bed column performance was obtained at high fixed bed depth, low effluent flow rate, and low initial concentration. Successful desorption and regeneration were achieved with 0.2 M HCl and 0.1 M NaOH. BET, scanning electron microscopy, energy dispersive X-ray spectroscopy, and FTIR and X-ray photoelectron spectra analyses confirmed that ammonium removal was mainly ascribed to exchanging with sodium in the adsorbent, and phosphate adsorption mainly followed the surface complexion mechanism; the surface hydroxyl groups played the key role. All the results proved that the column could be promising option for the simultaneous removal of phosphate and ammonium at lower concentrations.

Keywords: Phosphate; Ammonium; Modified zeolite; Fixed-bed column; Mechanism

1. Introduction

It is generally recognized that the presence of phosphate in waters, such as lake, reservoirs, or rivers and the enclosed coastal areas, can trigger their eutrophication, resulting in excessive growth of algae and aquatic plants, with a consequent increase in dissolved oxygen depletion and fish toxicity [1–3]. Therefore, many countries and regions struggle to reduce

*Corresponding author.

the concentration of phosphate as much as possible. However, recent studies have indicated that ammonium could be the limiting factor for lake eutrophication during seasonal variations [4,5]. Consequently, the practice of simultaneous management of phosphate and ammonium input to water bodies has received great attention from many researchers [6,7]. At present, technologies including chemical precipitation [8], biological treatment [9], adsorption [10,11], membrane filtration [12], and constructed wetland [13] have been used to remove phosphate and ammonium from municipal wastewater. Among these various treatment processes, adsorption is recommended as an attractive option removal method for the low concentrations of phosphate and ammonium, owing to its flexibility and simplicity of design, ease of operation, and economic advantages [14].

Recently, there is a growing trend in using low-cost and environmental friendly adsorbents for phosphate and ammonium removal. In this context, there are several adsorbents that prepared from natural minerals have been studied, such as bentonite [1], attapulgite [2], exfoliated vermiculite [15], tourmaline [16], fly ash [17], kaolinite [18], mesoporous silicates [19], and zeolite [20]. It has been found that modified zeolites had been widely used as effective adsorbents for ammonium and phosphate removal according to their mechanical and thermal properties, capability of cation exchange, and easy impregnation of active binding sites for anions [21].

Theoretically, increasing the cation exchange capacity of zeolites will average their affinity for ammonium. With this aim, salt and thermal treatment was frequently used to improve the CEC of zeolites and thus enhance their adsorption performance with respect to ammonium [2]. However, zeolites have been rarely used for phosphate adsorption due to the constant negative charge on their surface. Until now, many studies have revealed that metal oxide incorporation or impregnation was an effective method to boost the phosphate adsorption capacities of adsorbents [15]. In particular, as compared to calcium, aluminum, or iron, lanthanum-modified adsorbents particularly demonstrate several promising advantages during phosphate removal, such as their superior adsorption capacity, wide operating pH range, and high removal rate at low phosphate concentrations.

Although many studies have employed modified zeolites as ammonium and phosphate adsorbents, most of them were investigated for the effects of adsorption conditions, adsorption kinetics, and equilibrium via batch procedures; very few reports have dealt with their application under continuous adsorption conditions in laboratory-scale. However, the dynamic adsorption systems have significant advantages, such as treating large volume of wastewater, easy scale-up from laboratory-scale processes, simple operation, and reduced requirement of adsorbents. Thus, it is imperative to analyze continuous adsorption data, which can provide valuable information for improving the design and operation of phosphate and ammonium adsorption process from wastewater treatment plants.

Meanwhile, the batch study results of phosphate and ammonium adsorption by NaCl–Thermal–$LaCl_3$ synthetic modified zeolite (SMZ) were found to be encouraging; it had been aimed that the SMZ-packed fixed-bed column parameters on phosphate and ammonium removal from simulated municipal wastewater should be investigated prior designing the pilot scale filter for field test.

Consequently, as the continuation of our previous research, we focused on evaluating the applicability of NaCl–Thermal–$LaCl_3$ SMZ for removing phosphate and ammonium simultaneously from simulated municipal wastewater in fixed-bed column. The specific objectives of this study are as follows: (1) to investigate the effects of process parameters and to determine the dynamic adsorption capacity of SMZ, (2) to apply mathematical models including Adams–Bohart, Thomas, Yoon–Nelson, and bed depth service time (BDST) in describing experimental data, (3) to examine the reusability of SMZ, and (4) to reveal the simultaneous adsorption mechanism of phosphate and ammonium by FTIR and XPS analysis.

2. Materials and methods

2.1. Preparation of adsorbent

To develop phosphate and ammonium adsorbents, this study employed zeolite as substrate and soaked in NaCl solution for activation and $LaCl_3$ solution as the loading active binding. Firstly, 10.0 g of original zeolite was added to 200 mL aqueous solution containing 4 g NaCl in 500 mL beaker, stirring at the rate of 200 rpm for 6 h. Then, the NaCl-modified zeolite was calcinated at 400℃ for 30 min in muffle furnace. Afterward, the previously roasted zeolite was added into the prepared $LaCl_3$ solution (0.4%), adjusting the pH of the mixture to 10.0 by 1 mol/L NaOH and HCl solution. The mixture was kept stirring at the speed of 200 rpm for 6 h at the room temperature. This procedure led to the La deposition onto the surface of zeolite. Finally, the SMZ was washed with DI water until the supernatant was pH neutral and dried at 383 K for 24 h.

2.2. Experimental methods

2.2.1. Column adsorption test with simulated solution

The fixed-bed column adsorption tests were conducted in polyethylene tube with an internal diameter of 2 cm and height of 30 cm. SMZ particles were packed into the column using the "slurry method." The column was first filled with glass beads (2 cm) at the bottom to produce an even flow. It was then packed with SMZ, followed by another layer of glass beads and a piece of sponge to prevent SMZ from seeping out with the effluent. A certain amount of SMZ (20, 40, 60 g) was packed into the column to achieve the desired bed height (2, 4, and 6 cm). The input solution containing various phosphate and ammonium concentrations (2.5–10, 5–20, 10, and 40 mg/L) was pumped upward through the column at different flow rates (10, 15, and 20 mL/min) by peristaltic pumps. Effluent samples were collected at definite intervals of time in 20-mL plastic tubes for the determination of the phosphate and ammonium concentrations. Fig. 1 presented the schematic diagram of the SMZ fixed-bed column.

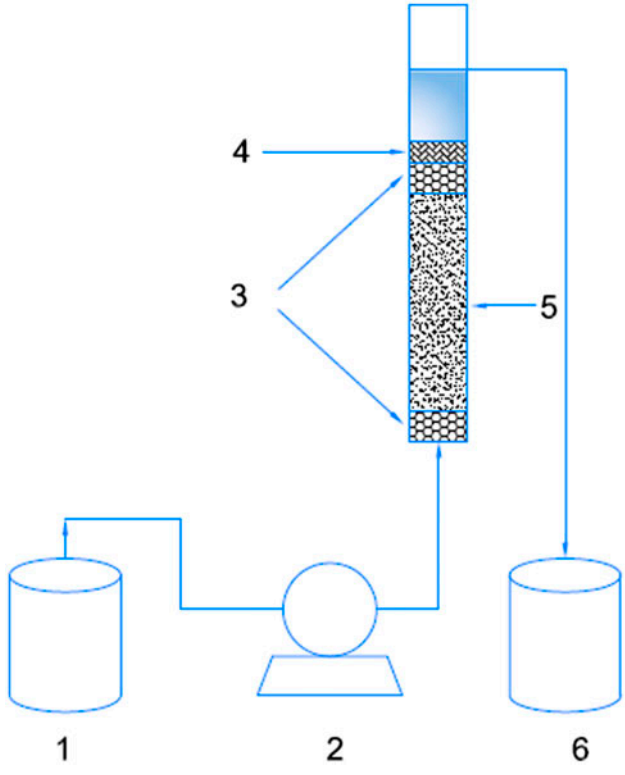

Fig. 1. The schematic diagram of laboratory-scale mini-column tests.
Notes: (1) feed tank, (2) peristaltic pump, (3) glass beads, (4) sponge pad, (5) SMZ bed, and (6) effluent storage tank

The breakthrough time (t_b) and treated volume at breakthrough time (V_b) are determined as the time and volume when the effluent phosphate or ammonium concentration (C_t) reached 10% of the influent concentration ($C_t/C_0 = 0.10$). Similarly, the exhaustion time (t_e) and treated volume at exhaustion time (V_e) are defined as the time and volume when the effluent phosphate or ammonium concentration (C_t) reached 90% of the influent concentration ($C_t/C_0 = 0.90$). The total amount of phosphate or ammonium adsorbed onto SMZ column, q_{total} (mg) and the dynamic adsorption capacity, q_e (mg/g) are calculated according to the following equations:

$$q_{total} = \frac{Q}{1000}\int_0^{t_{total}} C_{ad}\, dt \quad (1)$$

$$q_e = \frac{q_{total}}{m} \quad (2)$$

where t_{total}, Q, m, and C_{ad} are the total time for the column to reach saturation (min), volumetric flow rate (mL/min), the amount of SMZ packed in the column (g), and the difference in the phosphate or ammonium concentration at the initial time and the t time caused by adsorption (mg/L), respectively.

2.2.2. Desorption and regeneration tests

Desorption and regeneration were performed with the same column as above. Prior to desorption, phosphate- and ammonium-adsorbed SMZ was rinsed with 1 L distilled water at the flow rate of 10 mL/min to remove residual phosphate and ammonium. Then, 0.2 M HCl solution was pumped upward through the column at flow rate of 10 mL/min. The desorbed SMZ column was washed with 1,000 mL of distilled water at a flow rate of 20 mL/min. Then, it was reactivated with 1,000 mL of 0.1 M NaOH at a flow rate of 10 mL/min. After that, it was washed with 1,000 mL of distilled water at a flow rate of 20 mL/min. The regenerated SMZ column was reused for the next cycle of adsorption–desorption. Three cycles have been implemented successively.

2.3. Analytical methods

Specific surface area, total pore volume, and average pore size (BET) were evaluated by the gas nitrogen adsorption method (ASAP2010M+C, Micrometrics Inc. USA).

Surface morphology and chemical compositions of the absorbent were determined by scanning electron

microscopy (SEM, ZEISS-EVO18, Germany) and energy dispersive X-ray spectroscopy (EDS, INCA ENERGY 350, UK).

FTIR spectra were collected on Nicolet IS10 FTIR spectrophotometer (Thermo scientific, USA) using transmission model from 400 to 4,000 cm^{-1}. Samples for FTIR determination were ground with spectral grade KBr in an agate mortar.

X-ray photoelectron spectra (XPS) were collected on an ESCALab-220i-XL spectrometer with monochromatic Al-Kα X-ray source. For wide scan spectra, an energy range of 0–1,100 eV was used with pass energy 80 eV and step size 1 eV. The high-resolution scans were conducted according to the peak being examined with pass energy 40 eV and step size 0.05 eV. The XPS results were collected in binding energy forms and fitted using a nonlinear least squares curve-fitting program (XPSPEAK41 Software).

2.4. Modeling of breakthrough curves

The bed volume of breakthrough and the shape of breakthrough curves are important characteristics for determining the operation and dynamic response of an adsorption column. Furthermore, the successful design of an adsorption column requires the prediction of the concentration–time profile from the breakthrough curve for the effluent discharged from the column. Breakthrough curves models, including Thomas, Yoon–Nelson, Adams–Bohart, and BDST models, were fitted to experimental data using linear regression methods. Relative parameters and constants were calculated.

3. Results and discussion

3.1. Effect of column design parameters

3.1.1 Effect of influent pH

The solution pH could be critical influencing factor to the dynamic adsorption process since it can affect ionic state of the functional groups and phosphate and ammonium species as well. The effect of influent pH on phosphate and ammonium removal by SMZ column was examined at pH values of 4, 6, and 8, while keeping the constant initial phosphate and ammonium concentration (p = 5 mg/L, N = 20 mg/L), bed depth (2 cm), and flow rate(10 mL/min).

As can be seen from Fig. 2, the ammonium adsorption capacity by SMZ-packed column increased from 9.91 to 10.60 mg/g with the solution pH rising from 4 to 6, while it declined to 9.08 mg/g at pH 8 (Table 1). It implied that the breakthrough happened more slowly at pH 6 for ammonium adsorption. These findings agreed well with those of the batch adsorption test in the previous study. This can be explained by the change in density of hydrogen ions, the dominant ionic species of ammonium, and the surface charge of SMZ as the function of solution pH. According to the relation of ammonium dissociation as the function of pH, NH_4^+ is the dominant species in solution at the pH below 7, while the partial of ammonium transforms into electrically neutral NH_3 at alkaline pH [22]. By considering the above facts, the increase in breakthrough time of ammonium with solution pH from 4 to 6 can be attributed to decrease in hydrogen ions in solution, and thus reduction of the competition of hydrogen ions with ammonium ions for adsorption sites onto zeolite particles [23]. The decrease in adsorption capacity for ammonium adsorption at pH

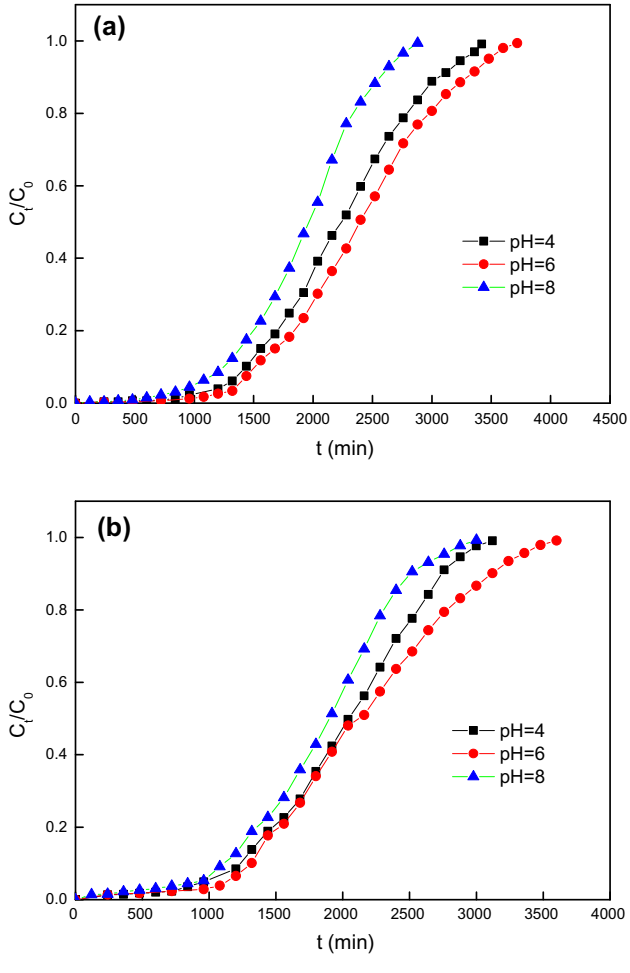

Fig. 2. Effect of solution pH on the breakthrough curve of phosphate (a) and ammonium (b) adsorption onto SMZ (bed depth of 4 cm, flow rate of 10 mL/min, input concentration of 5 mg/L-P and 20 mg/L-N).

Table 1
Breakthrough curves parameters for the adsorption of phosphate and ammonium onto SMZ at different operating conditions

Experimental conditions	pH	H (cm)	Q (mL/min)	C_0 (mg/L)		T_b (min)		Q_b (mg/g)		T_s (min)		Q_s (mg/g)		MTZ (cm)	
				P	N	P	N	P	N	P	N	P	N	P	N
pH	4	4	10	5	20	1,440	1,200	1.76	4.96	2,940	2,730	2.67	9.91	2.04	2.24
	6	4	10	5	20	1,620	1,320	1.84	5.80	3,480	3,120	2.99	10.60	2.14	2.31
	8	4	10	5	20	1,260	960	1.53	4.67	2,580	2,520	2.37	9.08	2.05	2.48
Bed depth	6	2	10	5	20	720	540	1.70	2.59	1,560	1,440	2.72	8.96	1.08	1.25
	6	4	10	5	20	1,620	1,320	1.84	5.80	3,480	3,120	2.99	10.60	2.14	2.31
	6	6	10	5	20	2,580	2,160	2.05	6.90	5,760	5,280	3.52	11.39	3.31	3.55
Flow rate	6	4	10	5	20	1,620	1,320	1.84	5.80	3,480	3,120	2.99	10.60	2.14	2.31
	6	4	15	5	20	760	740	1.39	4.03	2,100	1,800	2.51	9.08	2.55	2.36
	6	4	20	5	20	440	420	1.02	3.58	1,320	1,260	2.19	7.93	2.67	2.67
C_0	6	4	10	2.5	10	2,640	2,160	1.60	5.17	5,760	5,260	2.60	8.83	2.17	2.36
	6	4	10	5	20	1,620	1,320	1.84	5.80	3,480	3,120	2.99	10.60	2.14	2.31
	6	4	10	10	40	870	720	2.12	6.90	1,830	1,740	3.34	11.77	2.10	2.34

8 was probably due to the increase in percentage of molecular ammonium, which resulted in the decrease of ion exchange potential.

As for phosphate adsorption, the higher adsorption capacity was obtained from pH 4–6, indicating that the lanthanum incorporation onto the SMZ surface works as active sites by providing the greater affinity to the monovalent phosphate species ($H_2PO_4^-$) and the protonated form of La $(OH)_2^+$ could be easier to be displaced at low pH from metal-binding sites than hydroxyl groups which can facilitate the ligand exchange process [24]. The decrease in adsorption capacity observed at pH 8 was probably ascribed to the more negative charges on the adsorbent surface with the de-protonation of active sites as well as the competitive adsorption between HPO_4^{2-} and increasing amounts of OH^-. Moreover, the high concentration of OH^- in high pH solution hindered the occurrence of ligand exchange between phosphate species and hydroxyl groups, thus reducing the adsorption capacity of SMZ [25]. These results indicated that phosphate is mainly removed by ligand exchange and partly by electrostatic adsorption.

3.1.2. Effect of bed depth

The effect of bed depth on phosphate and ammonium adsorption by SMZ was explored with various bed depths (2, 4, and 6 cm), a constant initial concentration of phosphate (5 mg/L) and ammonium (20 mg/L), flow rate(10 mL/min). Fig. 3 shows that both the breakthrough and exhaustion time were extended with the increase in bed depth, which may be due to the longer bed depth allowing the solute to diffuse more into the interior of the adsorbent bed. Meanwhile, the slope of the breakthrough curves became flatter with the increase in bed depth indicated that the longer column took a longer time to reach complete exhaustion. The phosphate and ammonium adsorption capacity of SMZ columns was 2.72, 2.99, 3.52 mg/g and 8.96, 10.60, 11.39 mg/g, respectively, for the bed depth of 2, 4, and 6 cm (Table 1). This increasing tendency could be attributed to the availability of more binding sites for adsorption and an increase in the contact time between the adsorbent and adsorbate [26]. These results are in agreement with the findings of similar studies reported [27,28].

3.1.3. Effect of flow rate

To investigate the effect of varied flow rate (10, 15, 20 mL/min), the bed depth (4 cm) and initial concentration of phosphate (5 mg/L) and ammonium (20 mg/L) were maintained the same. As seen from Fig. 4, the shorter breakthrough time occurred at the higher flow rate for both phosphate and ammonium adsorption. As flow rate increased from 10 to 20 mL/min, the adsorption capacity decreased from 2.99 to 2.19 mg/g (Table 1). This can be explained by the fact that the higher flow rate results in the larger volume of water elapsed through the bed. As a consequence, more phosphate and ammonium ions contact with binding sites of SMZ, making them get saturated more quickly. Similarly, higher adsorption capacity was

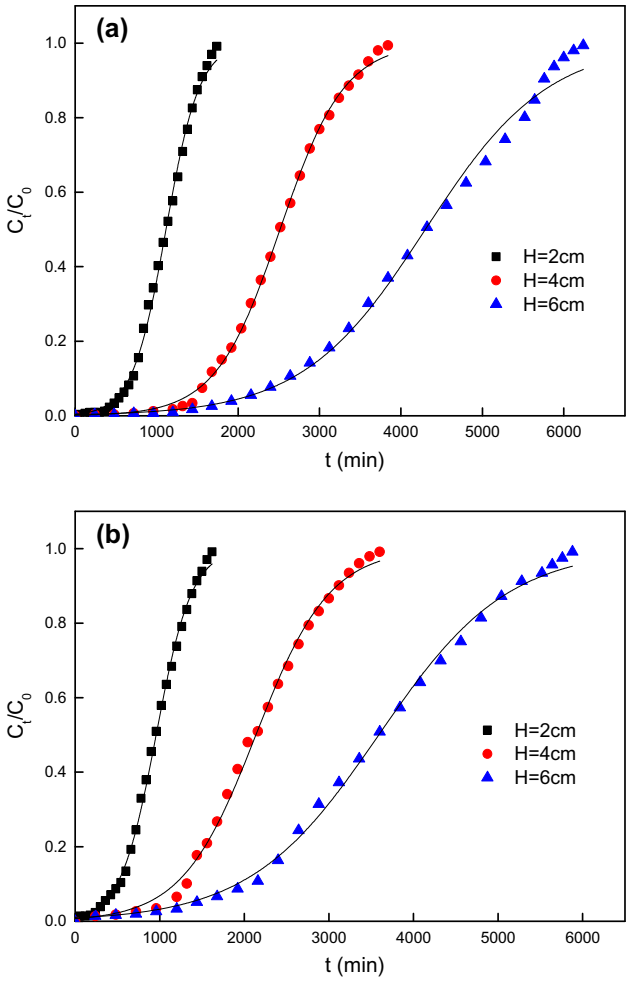

Fig. 3. Effect of bed depth on the breakthrough curve of phosphate (a) and ammonium (b) adsorption onto SMZ (pH of 6, flow rate of 10 mL/min, influent concentration of 5 mg/L-P and 20 mg/L-N).

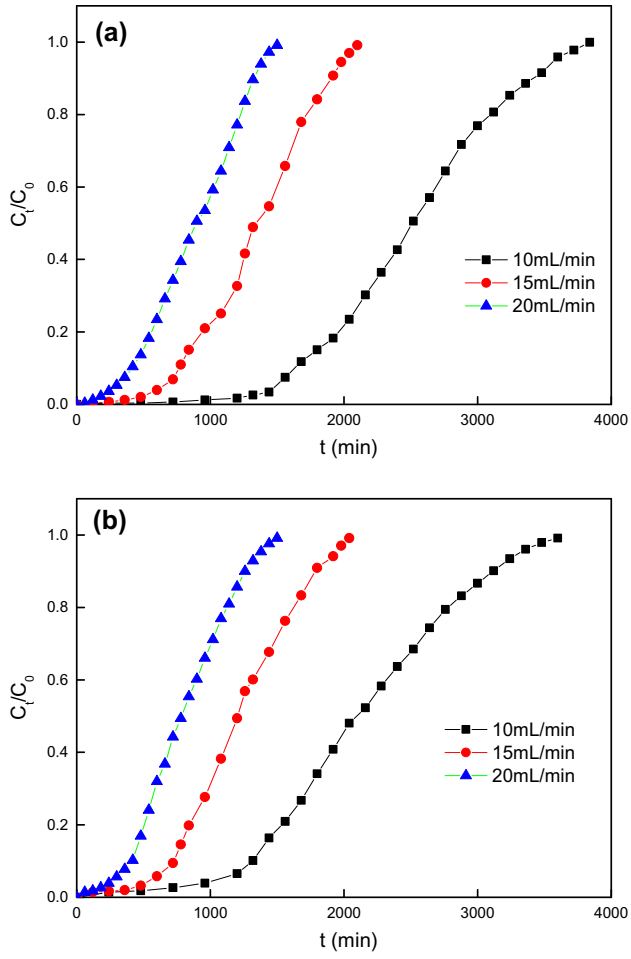

Fig. 4. Effect of flow rate on the breakthrough curve of phosphate (a) and ammonium (b) adsorption onto SMZ (pH of 6, bed depth of 4 cm, influent concentration of 5 mg/L-P and 20 mg/L-N).

obtained at lower flow rate. When the flow rate decreased, the contact time between phosphate, ammonium, and SMZ is longer, the intraparticle diffusion then becomes effective, and the equilibrium could be reached before ions moved out of the column [29]. Similar phenomena have been observed by other researchers [30,31]. Another explanation for decrease in the specific capacity of SMZ with the increase in flow rate can be the increased maldistribution or channeling at relatively higher flow rate in the column [32].

3.1.4. Effect of influent concentration of P and N

The effects of initial concentration on the breakthrough curves was examined in the range of 2.5–10 mg/L for phosphate and 10–40 mg/L for ammonium at the flow rate 10 mL/min and bed depth of 4 cm. As shown in Fig. 5, the adsorption process reached saturation faster, and the breakthrough time declined with the increase in influent concentration. As expected, the adsorption capacity increased with the increase in influent concentration. The dynamic adsorption capacity of SMZ for both phosphate and ammonium increased, from 2.60 to 3.34 mg/g and 8.83 to 11.8 mg/g, respectively, with the elevating influent concentration. This might be attributed to the fact that the higher concentration gradient caused greater driving force for the transport process to overcome mass transfer resistance [33]. As the influent concentration of phosphate and ammonium increases, the exhaustion time decreased for both of them. These results demonstrated that the higher initial

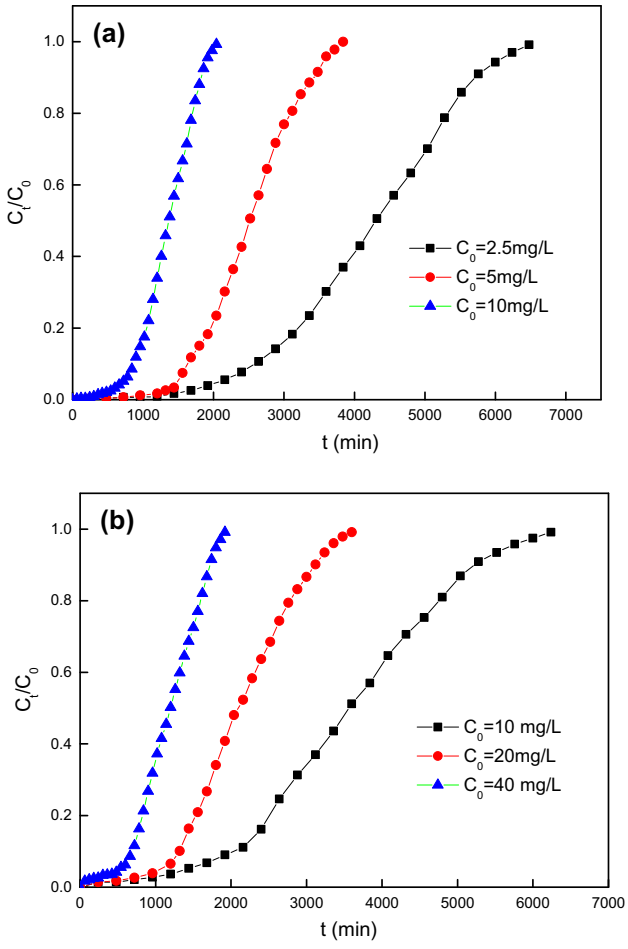

Fig. 5. Effect of influent concentration on the breakthrough curve of phosphate (a) and ammonium (b) adsorption onto SMZ (pH of 6, bed depth of 4 cm, flow rate 10 mL/min).

concentration caused the faster mass transfer, resulting in a decrease in the exhaustion time and adsorption zone length [34].

3.2. Breakthrough curve modeling

3.2.1. Adams–Bohart model

Adams–Bohart model is based on the assumption that the rate of the adsorption reaction is proportional to the residual active sites of adsorbent and concentration of adsorbate. That is, the rate of the adsorption is proportional to the fraction of adsorption capacity of the adsorbent still remains on the adsorbent. The equation of Adams–Bohart can be expressed as follows:

$$\ln \frac{C_t}{C_0} = K_{AB} C_0 \, t - K_{AB} N_0 \, \frac{Z}{F} \tag{3}$$

where C_0 and C_t (mg/L) are the influent and effluent concentrations; K_{AB} (L/mg min) is the kinetic constant; N_0 (mg/L) is saturation concentration of the column; Z (cm) is the bed depth; F (cm/min) is the linear velocity achieved by dividing the flow rate (cm^3/min) by the column section area (cm^2).

For all breakthrough curves using linear regression analysis, the respective values of K_{AB} and N_0 were calculated along with the correlation coefficients and listed in Tables 2 and 3. The adsorption capacity of the bed (N_0) decreased with the increase in flow rate but increased with influent concentration and bed depth. The kinetic constant of K_{AB} decreased with the increase in both bed depth and influent concentration; however, it increased with the increase in flow rate, indicating that the overall system kinetics was dominated by external mass transfer in the initial part of adsorption in the column. These results suggested that better adsorption performance of the column, characterized by higher adsorption capacity and lower kinetics, could be achieved with higher bed depth and influent concentration, but lower flow rate.

3.2.2. Thomas model

Thomas model assumed that the adsorption is not limited by chemical interactions but by mass transfer at the interface, and the experimental data follow Langmuir isotherms and second-order kinetics. Thomas model is appropriate for depicting the whole breakthrough curve. This model can be written in the linear form by the following equation:

$$\ln\left(\frac{C_0}{C_t} - 1\right) = K_{Th} q_0 \frac{m}{Q} - K_{Th} C_0 t \tag{4}$$

where K_{Th} stands for Thomas rate constant (mL/min mg), q_0 is the adsorption capacity (mg/g), C_0 is the inlet concentration (mg/L), C_t is the outlet concentration at time t (mg/L), m is the mass of adsorbent (g), Q is the feed flow rate (mL/min), and t is the filtration time (min). The values of K_{Th} and q_0 were determined from the linear plot of ln $(C_0/C_t - 1)$ against t and shown in Tables 2 and 3.

The relative constants and coefficients were obtained from linear regression analysis according to Thomas model equation, and the results were presented in Tables 2 and 3. It can be noted that the increase in bed depth resulted in a decrease in K_{Th}, but an increase in adsorption capacity for both of phosphate and ammonium, which may be due to the increase of mass transport resistance and the axial dispersion. As the flow rate increased, the values of K_{Th}

Table 2
Adams–Bohart, Yoon–Nelson, and Thomas models parameters obtained under different experimental conditions using linear regression analysis for phosphate

Experimental conditions				Adam–Bohart model			Yoon–Nelson model			Thomas model		
H (cm)	Q (mL/min)	C_0 (mg/L) P	C_0 (mg/L) N	$K_{AB} \times 10^{-4}$ (L/mg min)	$N_0 \times 10^4$ (mg/L)	R^2	$K_{YN} \times 10^{-3}$ (min^{-1})	τ (min)	R^2	$K_{Th} \times 10^{-3}$ (L/mg min)	q_0 (mg/g)	R^2
2	10	5	20	7.20	1.13	0.935	5.40	1,107	0.987	1.08	2.76	0.987
4	10	5	20	3.40	1.30	0.943	2.90	2,472	0.945	0.58	3.09	0.945
6	10	5	20	2.00	1.40	0.937	1.50	4,092	0.985	0.30	3.41	0.985
4	10	5	20	3.40	1.30	0.943	2.90	2,472	0.945	0.58	3.09	0.945
4	15	5	20	5.60	1.06	0.904	4.50	1,326	0.982	0.90	2.49	0.982
4	20	5	20	6.40	0.98	0.853	5.50	878	0.964	1.10	2.10	0.964
4	10	2.5	10	4.00	1.04	0.931	1.50	4,143	0.987	0.75	2.59	0.987
4	10	5	20	3.40	1.30	0.943	2.90	2,472	0.945	0.58	3.09	0.945
4	10	10	40	3.10	1.38	0.910	4.40	1,378	0.997	0.44	3.45	0.997

Table 3
Adams–Bohart, Yoon–Nelson, and Thomas models parameters obtained under different experimental conditions using linear regression analysis for ammonium

Experimental conditions				Adam–Bohart model			Yoon–Nelson model			Thomas model		
H (cm)	Q (mL/min)	C_0 (mg/L) P	C_0 (mg/L) N	$K_{AB} \times 10^{-4}$ (L/mg min)	$N_0 \times 10^4$ (mg/L)	R^2	$K_{YN} \times 10^{-3}$ (min^{-1})	τ (min)	R^2	$K_{Th} \times 10^{-4}$ (L/mg min)	q_0 (mg/g)	R^2
2	10	5	20	1.45	4.35	0.914	5.30	918	0.986	2.65	9.18	0.986
4	10	5	20	0.65	4.95	0.886	2.50	2,149	0.984	1.25	10.75	0.984
6	10	5	20	0.04	5.34	0.925	1.40	3,638	0.981	0.70	12.12	0.981
4	10	5	20	0.65	4.95	0.886	2.50	2,149	0.984	1.25	10.75	0.984
4	15	5	20	1.20	4.39	0.899	4.30	1,224	0.983	2.15	9.18	0.983
4	20	5	20	1.45	3.90	0.863	5.50	812	0.986	2.75	8.12	0.986
4	10	2.5	10	0.80	3.94	0.911	1.40	3,524	0.991	1.40	8.81	0.991
4	10	5	20	0.65	4.95	0.886	2.50	2,149	0.984	1.25	10.75	0.984
4	10	10	40	0.60	5.38	0.915	4.10	1,175	0.970	1.03	11.76	0.970

increased, while the values of q_0 decreased. An increase in influent concentration led to an elevation in both K_{Th} and adsorption capacity. This may be attributed to the increase in mass transfer tendency with the increase in the influent concentration of phosphate and ammonium which enhanced the solute loading per unit active adsorption sites [35]. As a result, the saturation of the adsorbent sites also become faster, leading to the decrease in exhaustion volume and time. Additionally, it was found that the values of q_0 estimated using Thomas model are very close to the q_e values calculated from experimental results with varying bed depth, flow rate, and influent concentration conditions. Comparing the correlation coefficient (R^2) values for various models, it revealed that the Thomas model suitably described the SMZ adsorption process in the fixed-bed column where the process was not only regulated by internal and external diffusion [36].

3.2.3. Yoon–Nelson model

Yoon–Nelson model is based on the assumption that the rate of decrease in the probability of adsorption for each adsorbate molecule is proportional to probability of adsorbate adsorption and the probability of adsorbate breakthrough on the adsorbent. The linearized equation of model can be expressed as:

$$\ln\left(\frac{C_t}{C_0 - C_t}\right) = K_{YN}t - \tau K_{YN} \quad (5)$$

where C_0 and C_t (mg/L) are the influent and effluent concentrations, K_{YN} (min^{-1}) is the rate of constant, and τ (min) is the time required for 50% adsorbate breakthrough. The values of K_{YN} and τ can be calculated from the slope and the intercept of the linear plot of $\ln[C_t/(C_0 - C_t)]$ vs. t.

Different statistical parameters of the Yoon–Nelson were calculated and given in Tables 2 and 3. It is observed that the values of K_{YN} decreased with an increase in bed depth, while the corresponding 50% breakthrough time τ values are noticed to increase. Moreover, the values of K_{YN} are found to increase with the increase in both flow rate and influent concentration of phosphate and ammonium, whereas the τ values showed an opposite trend. These results could be explained by the faster saturation of column at higher flow rate and influent concentration. Similar trends were reported by other researchers [37]. The 50% breakthrough time predicted by the Yoon–Nelson model was quite similar to that obtained from experiments indicating that Yoon–Nelson model could describe the column adsorption of phosphate and ammonium well.

3.2.4. BDST model

The BDST model was developed by Hutchins, which based on the assumptions that the intraparticle mass transfer resistance and external film resistance are negligible. This model could be applied to estimating the design parameters of fixed-bed column data from the physical measuring the bed capacity at different breakthrough values. This BDST model can be presented by Eq. (6):

$$t = \frac{ZN_{BD}}{C_0 v} - \frac{1}{K_{BD}C_0}\ln\left(\frac{C_0}{C_b} - 1\right) \quad (6)$$

where t is the service time of column (h), Z is the bed depth (cm), C_0 is the influent concentration (mg/L), C_b is the effluent concentration at breakthrough point (mg/L), N_{BD} is the column adsorption capacity (mg/L), K_{BD} is the rate constant (L/(mg h)), and v is the linear flow velocity and is calculated by dividing the flow rate by the area of column (cm/min).

Fig. 6 shows the plot of the service time vs. bed depth for phosphate and ammonium adsorption onto SMZ at 10, 30, 50, and 90% breakthrough time under constant flow rate (10 mL/min) and influent concentration (P 5 mg/L and N 20 mg/L). The values of K_{BD}, $N_{BD,}$ and R^2 were calculated from the slope (m) and intercept (C) of these plots. As seen from Table 4, the adsorption capacity N_{BD} slightly decreased with the bed depth, whereas the rate constant K_{BD} increased significantly. The high correlation coefficient (R^2) values demonstrated the applicability of the BDST model for predicting the service time of the adsorbents used in the dynamic adsorption.

The adsorption zone, known as mass transfer zone (MTZ), can be defined as the adsorbent layer through which the effluent concentration changes from 10 to 90% of the influent concentration. MTZ is identified as the horizontal distance between these two lines in the BDST plot. From Fig. 6, the MTZ in this study was estimated to be 3.80 cm for phosphate and 4.25 cm for ammonium. The length of the MTZ was found to increase with the increase in bed height and flow rate for both phosphate and ammonium. Another noteworthy finding was that the linear regression of 50% breakthrough did not pass through the origin. Theoretically, the 50% breakthrough should be a straight line pass through the origin at $t = 0$ h [31]. This nonconformity indicated that the transport of phosphate and ammonium from the aqueous solution onto the SMZ involves more than one rate-limiting step. The constants obtained from the BDST model can be useful for the theoretical predictions of scaling up the process for other flow rates and influent concentration conditions [38].

3.3. Dynamic adsorption capacity of SMZ

The dynamic adsorption capacity of SMZ for phosphate and ammonium at the breakthrough time and exhaustion time was calculated for different operating conditions and summarized in Table 1. The highest adsorption capacity of SMZ for phosphate and ammonium at the exhaustion time was 3.52–11.77 mg/g, accounting for 39.23 and 5.88 times of natural zeolite adsorption capacity. This maximum value was achieved for a bed height of 6 cm, flow rate of 10 mL/min and initial phosphate and ammonium concentration of 40 and 10 mg/L, and influent pH of 6. The result indicated that SMZ can simultaneously and effectively remove phosphate and ammonium in the continuous adsorption systems. The reasonably high adsorption capacity of SMZ column for phosphate can be explained by the fact that La oxide loading resulted in the development of effective binding sites for phosphate anions on the surface of zeolite. The high capacity for ammonium was ascribed to the NaCl–thermal activation, which could enhance the cation exchange capacity of zeolite. Consequently, the retention of phosphate and ammonium onto SMZ was strengthened.

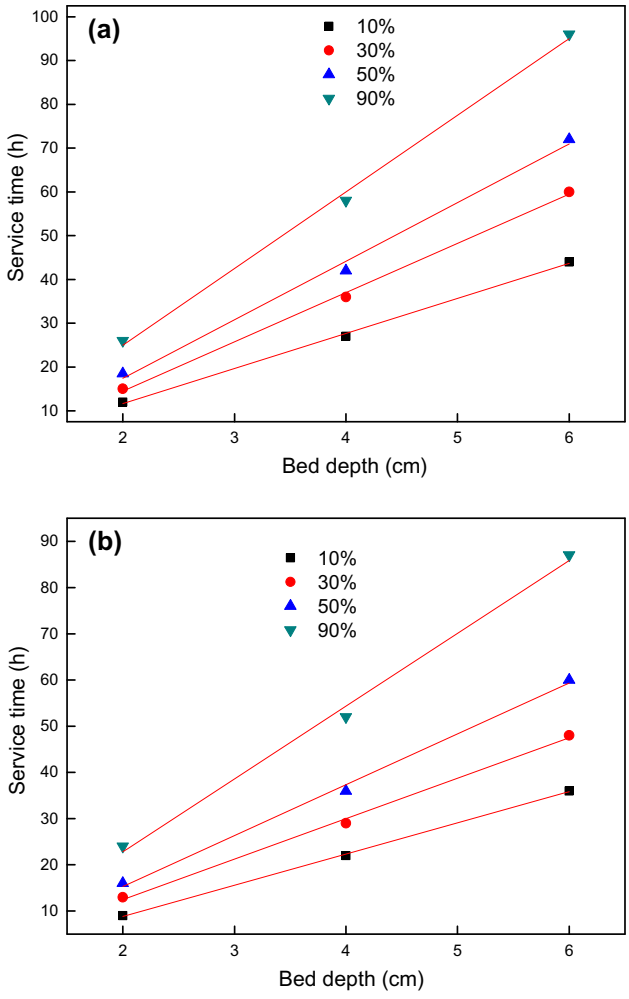

Fig. 6. BDST model for 10, 30, 50, and 90% breakthrough at different bed depths and constant flow rate (10 mL/min) and influent concentration of 5 mg/L-P and 20 mg/L-N.

3.4. Desorption and regeneration

Desorption and regeneration play a critical role in sustainable use of the adsorbent. Reusability of any adsorbent can be evaluated by its adsorption performance in successive adsorption–desorption cycles. In our batch adsorption tests, the dilute acid solution following the alkaline solution (0.2 M HCl and 0.1 M NaOH) was proven to be the best desorption solution. In this study, 0.2 M HCl and 0.1 M NaOH were employed for eluting phosphate and ammonium from saturated SMZ column. Prior to desorption test, phosphate- and ammonium-saturated SMZ column was washed with an abundant amount of distilled water to eliminate unbound phosphate and ammonium.

The values of breakthrough time, exhaustion time, and adoption capacity for all three cycles were presented in Table 5. It was found that phosphate and ammonium adsorption capacity in the first cycle was 9.96 and 2.31 mg/g, and then it gradually decreased to 9.02 and 1.51 mg/g, which was approximately 50–85% of initial adoption capacity. The results indicated that the increasing adsorption cycles may destroy the binding site on the surface of SMZ, leading to the capacity loss for phosphate. After three cycles of operation, the adsorption capacity of SMZ column was 1.05–9.02 mg/g for phosphate and ammonium, respectively, indicating that the adsorbent could be reused for at least three cycles. The elution of phosphate and ammonium from SMZ column might result from ligand/ion exchange reaction, whereby OH^- ions from NaOH displaced phosphate ions from the surface of SMZ and H^+ from HCl exchanged NH_4^+ ions.

3.5. Performance indicator

Performance of fixed-bed columns is basically indicated by the number of bed volumes (BVs) treated before the breakthrough point and adsorption exhaustion rate (AER). Higher the number of BV before the breakthrough point, the better will be the column performances [39]. Number of the BVs treated before breakthrough can be calculated by the following relation:

$$\mathrm{BV} = \frac{\text{Volume of water treated at breakthrough point (L)}}{\text{Volume of adsorbent bed (L)}} \tag{7}$$

Table 4
BDST model constants estimated for adsorption of phosphate and ammonium onto SMZ using linear regression analysis

	m (h/cm)		C (h)		N_{BD} (mg/cm^3)		$K_{BD} \times 10^{-1}$ (L/mg h)		R^2	
C/C_0 (%)	P	N	P	N	P	N	P	N	P	N
10	8.00	6.75	−4.33	4.67	7.60	25.8	1.01	0.24	0.997	0.999
30	11.3	8.75	−8	5.00	10.8	33.4	0.21	0.08	0.997	0.995
50	13.4	11.0	−9.33	6.67	12.8	42.0	0.008	0.003	0.990	0.994
90	17.5	15.8	−10	8.67	16.7	60.4	−0.44	−0.13	0.995	0.992

Table 5
Phosphate and ammonium adsorption–desorption parameters for three cycles

	V_b (L)		V_e (L)		m_b (mg/g)		m_e (mg/g)	
Cycle number	P	N	P	N	P	N	P	N
1	10.2	4.8	28.4	13.2	1.35	5.22	2.31	9.96
2	7.2	3.6	14.8	11.4	0.96	4.65	1.51	9.02
3	3.6	3.6	9.6	9.0	0.04	3.98	1.05	9.02

During continuous flow operation, the adsorbent is gradually exhausted. The rate of exhaustion is defined as the mass of adsorbent deactivated per unit volume of water treated at exhaustion point. The value of AER can be given by the equation:

$$\text{AER} = \frac{\text{Mass of adsorbent (g)}}{\text{Volume of water treated (L)}} \quad (8)$$

Values of BV and AER calculated from the experimental data for the present system are shown in Table 6, which suggested that the treated BV increased with the increase in fixed bed depth, decreasing the rate of effluent discharge and lessening of C_0 in feed water. Meanwhile, the decrease in AER indicated the enhancement of fixed-bed columns performances. As the AER value reduced with the increase in fixed bed depths, decrease in effluent discharge rate, and decrease in C_0 for the present system, it can be said that the SMZ fixed-bed column displayed well the performance of phosphate and ammonium simultaneous removal. Although the phosphate and ammonium removal capacity noted to be higher for the higher influent concentration, but the exhaustion rate of fixed-bed column was faster than the other lower influent concentrations used in this experiment indicating the decrease in column performance.

3.6. Proposed P and N removal mechanism on SMZ

3.6.1. BET study on SMZ before and after adsorption

BET results show that the specific surface area, total pore volume, and mean pore diameter of SMZ were 42.91 m^2/g, 0.058 cm^3/g, and 10.85 nm, respectively, whereas these values after adsorption were 38.48 m^2/g, 0.05 cm^3/g, and 12.71 nm, respectively. The specific surface area of the SMZ was slightly reduced after the adsorption of phosphate and ammonium as consequence of the interaction between phosphate and lanthanum oxide that impregnated on the surface of zeolite [6], confirming that the chemisorption of phosphate occurred.

3.6.2. SEM-EDS study of SMZ before and after adsorption

The SEM images obtained from the SMZ before and after the adsorption of ammonium and phosphate are shown in Fig. 7. The SEM image showed that ammonium and phosphate were adsorbed by zeolite with more spherical particles distributed on the surface, and a number of protuberances formed a stacking structure. The particle morphology on SMZ had changed; this should be due to the adsorption of phosphate which crystallized on the active sites that increase the particle size. Corresponding EDS analyses demonstrated that the spherical clusters consisted mainly of La, Na, P, O, N, Si, and Al, thereby indicating a possible La−P complex formation. On the other hand, the weight percentage of Na^+ decreased from 2.49 to 0.86%, respectively, after the adsorption of ammonium and phosphate. The presence of N and observed reduction confirmed that the exchange of Na^+ and K^+ with ammonium was the main mechanism involved.

3.6.3. FTIR study on SMZ before and after adsorption

The FTIR spectra of SMZ before and after the adsorption of ammonium and phosphate are shown in Fig. 8. After the adsorption of ammonium, new peak appeared at 1,400 cm^{-1}, which corresponded to the symmetric bending vibrations of N−H, thereby indicating that the removal of ammonium onto SMZ was mainly via chemisorption. The presence of NH_4^+ was mainly attributed to the exchange ability of Na^+ and Ca^{2+} in SMZ would exchange with NH_4^+ in the solution, thereby causing the retention on SMZ. FTIR spectra in the region where v is 1,200–800 cm^{-1} could be used for the structural determination of the phosphate complexes on the metal oxides [40]. The phosphate

Table 6
The SMZ column performance indicators at different experiment conditions

	Bed depth (cm)						Flow rate (mL/min)						Input concentration (mg/L)					
	2	4			6		10		15		20		P:2.5; N:10		P:5; N:20		P:10; N:40	
Parameters	P	N	P	N	P	N	P	N	P	N	P	N	P	N	P	N	P	N
Treated BV ($\times 10^3$)	1.15	0.86	1.29	1.05	1.40	1.15	1.29	1.05	0.90	1.75	0.57	1.34	2.01	1.62	1.29	1.05	0.69	0.55
AER (g/L)	1.28	1.39	1.15	1.28	1.04	1.14	1.15	1.28	1.43	1.48	1.59	1.67	0.69	0.76	1.15	1.28	2.18	2.30

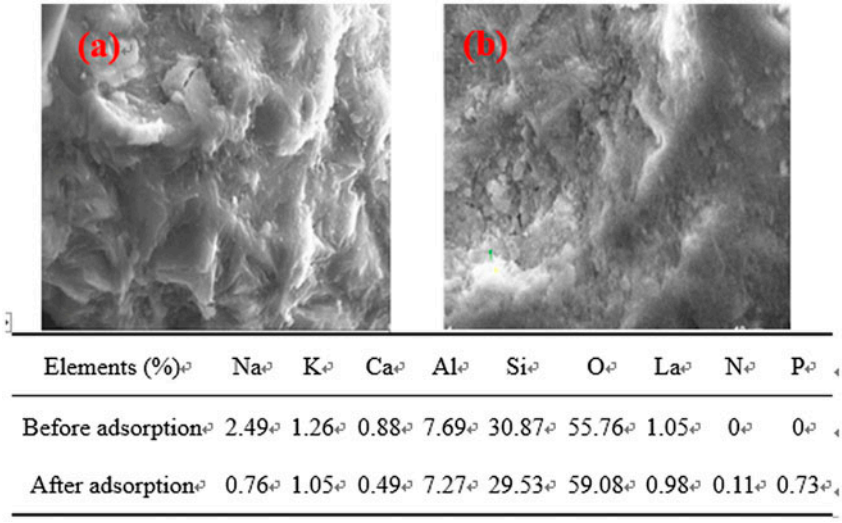

Elements (%)	Na	K	Ca	Al	Si	O	La	N	P
Before adsorption	2.49	1.26	0.88	7.69	30.87	55.76	1.05	0	0
After adsorption	0.76	1.05	0.49	7.27	29.53	59.08	0.98	0.11	0.73

Fig. 7. SEM images of SMZ before adsorption (a) and after adsorption (b) of phosphate and ammonium and corresponding EDS data.

surface complexes include $XOPO_3$ with C_v symmetry, $(XO)_2PO_2$ with C_{2v} symmetry, and $(XO)_3PO$ with C_{3v} symmetry (X=H or a metal atom), and each complex has its own characteristic FTIR bands. For the adsorption of phosphate, the FTIR spectra after adsorption appeared a novel and small broad weak band at $v = 1{,}068\ cm^{-1}$, which may be attributed to the typical characteristic of the asymmetric stretch vibration of P–O stretching mode [41]. Therefore, it was deduced that the surface of hydroxyl group of SMZ could be exchanged by the adsorbed phosphate. Based on its relative intensity, these results were consistent with the protonated monodentate complex $\equiv(LaO)(OH)PO_2$. Furthermore, at the pH 7 levels used in this study, the likely surface complex with the symmetry closest to C_{2v} is the protonated monodentate species $\equiv(LaO)(OH)PO_2$. To further confirm our above-mentioned analysis, FTIR studies on pure La_2O_3 with and without phosphate adsorbed were conducted. The results clearly showed that the new characteristic adsorption peak at $1{,}068\ cm^{-1}$ after pure La_2O_3 adsorbed phosphate. Our results are in good agreement with those of previous studies, which showed that the ligand exchange process at neutral pH on lanthanum oxide surfaces leads to the formation of protonated monodentate species [42].

3.6.4. XPS study SMZ before and after adsorption

To gain further insights into mechanism of ammonium and phosphate adsorption on SMZ, the XPS wide scan and surface O 1 s spectra of SMZ before and after ammonium and phosphate adsorption at pH 7 were analyzed and demonstrated in Figs. 9 and 10. It is clearly shown that N 1 s and P 2 p peaks in the spectra of adsorbed SMZ indicate the presence of N and P on the surface of the sample. The decrease in Na 1 s (1,060.12 eV) element content from 2.10 to

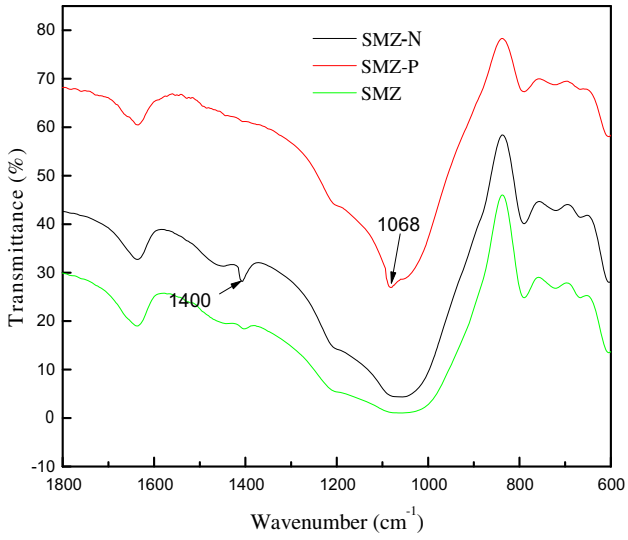

Fig. 8. FTIR spectra of SMZ, SMZ after adsorption of ammonium (SMZ-N), and phosphate (SMZ-P).

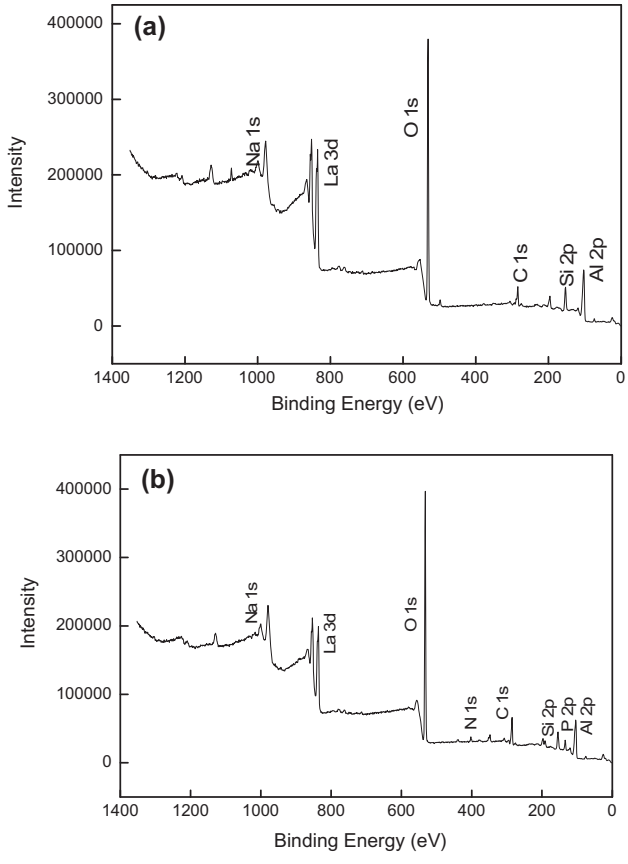

Fig. 9. XPS wide scan spectra of SMZ (a) before and (b) after adsorption of ammonium and phosphate.

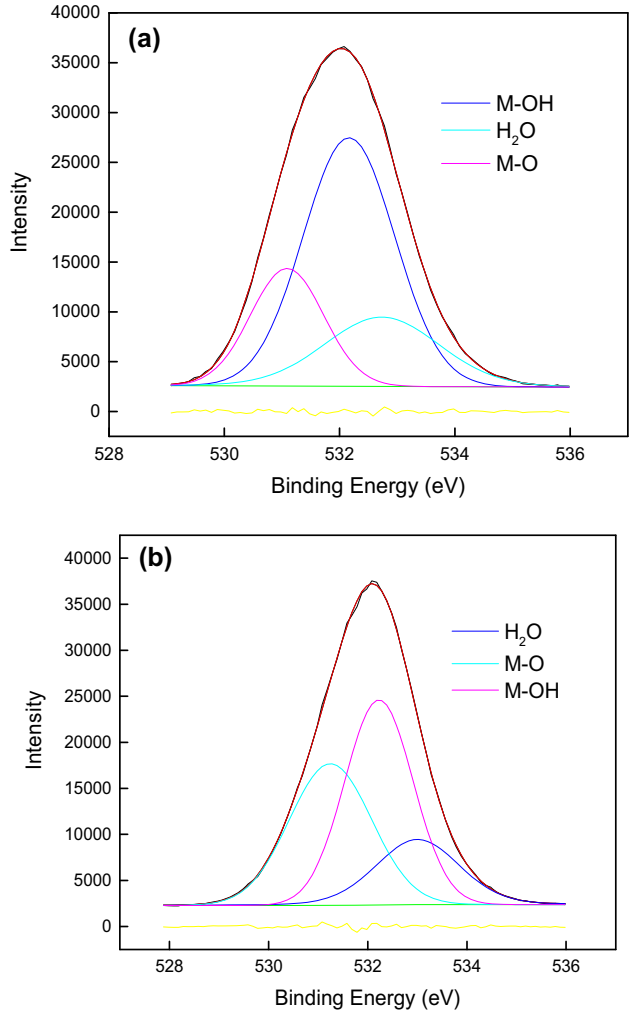

Fig. 10. XPS spectra of surface O 1 s of SMZ (a) before and (b) after adsorption of ammonium and phosphate.

1.22% (Table 7) may be due to the ion exchange of Na^+ with NH_4^+. Based on the binding energy of different oxygen species, the O 1 s XPS spectra were divided into three peaks with binding energy of 531.08–532.18 eV and 532.89 eV, which can be assigned to oxide oxygen (M–O) and hydroxyl group (M–OH) and adsorbed water (H_2O), respectively. After adsorption of N and P, the relative area ratio for the peak attributed to M–O increases from 20.78 to 37.17%, while the relative areas for the peak of M–OH decrease from 57.15 to 42.28%. The decrease in hydroxyl group percentage could be the replacement of –OH by phosphate during the adsorption process. Thus, the XPS analysis also suggested that the surface hydroxyl groups play the key role in the phosphate adsorption, which was in accordance with results of pH effect and FTIR studies.

Table 7
Atomic ratio of virgin SMZ and N–P-adsorbed SMZ by XPS study

Atomic ratio (%)	Si	Al	La	Na	O	N	P
Virgin SMZ	42.33	3.06	4.32	2.10	48.19	0	0
N–P-adsorbed SMZ	34.81	2.82	3.75	1.22	52.14	0.96	4.30

4. Conclusions

Investigation on the variable parameters such as solution pH, fixed bed depths, flow rate, and influent concentration for designing filter for phosphate and ammonium treatment suggested prospective results for using SMZ-packed fixed-bed columns. Experiment results revealed that an increase in bed depth and influent concentration or a decrease in flow rate improves the adsorption capacity for both phosphate and ammonium. Both Thomas and Yoon–Nelson models were found to describe well the breakthrough curves obtained under different experimental conditions. The breakthrough data at different fixed bed depths explained the BDST nicely, indicating SMZ could be used efficiently for phosphate and ammonium removal. Lower values of AER and larger values of BV were obtained at higher bed depth and lower flow rate and influent concentration, which suggested good performance. Desorption and regeneration of saturated SMZ column could be achieved with 0.2 M HCl and 0.1 M NaOH. BET, SEM-EDS, FTIR and XPS analyses confirmed that phosphate removal followed surface complex mechanism, and ammonium was mainly removed by ion exchange. The results proved that SMZ can be used as a promising phosphate and ammonium adsorbent in practical wastewater treatment.

Acknowledgment

The authors would like to appreciate the anonymous reviewers for their insightful comments and suggestions that significantly improved the manuscript. This work was financially supported by the National Natural Science Foundation of China (No. 51174017).

References

[1] M. Zamparas, M. Drosos, Y. Georgiou, Y. Deligiannakis, I. Zacharias, A novel bentonite-humic acid composite material Bephos™ for removal of phosphate and ammonium from eutrophic waters, Chem. Eng. J. 225 (2013) 43–51.
[2] H. Yin, M. Kong, Simultaneous removal of ammonium and phosphate from eutrophic waters using natural calcium-rich attapulgite-based versatile adsorbent, Desalination 351 (2014) 128–137.
[3] M.R. Awual, A. Jyo, T. Ihara, N. Seko, M. Tamada, K.T. Lim, Enhanced trace phosphate removal from water by zirconium(IV) loaded fibrous adsorbent, Water Res. 45 (2011) 4592–4600.
[4] W.M. Lewis, W.A. Wurtsbaugh, H.W. Paerl, Rationale for control of anthropogenic nitrogen and phosphorus to reduce eutrophication of inland waters, Environ. Sci. Technol. 45 (2011) 10300–10305.
[5] H.W. Paerl, H. Xu, M.J. McCarthy, G. Zhu, B. Qin, Y. Li, W.S. Gardner, Controlling harmful cyanobacterial blooms in a hyper-eutrophic lake (Lake Taihu, China): The need for a dual nutrient (N & P) management strategy, Water Res. 45 (2011) 1973–1983.
[6] D. Guaya, C. Valderrama, A. Farran, C. Armijos, J.L. Cortina, Simultaneous phosphate and ammonium removal from aqueous solution by a hydrated aluminum oxide modified natural zeolite, Chem. Eng. J. 271 (2015) 204–213.
[7] Z. Wang, H. Guo, F. Shen, G. Yang, Y. Zhang, Y. Zeng, L. Wang, H. Xiao, S. Deng, Biochar produced from oak sawdust by Lanthanum (La)-involved pyrolysis for adsorption of ammonium (NH_4^+), nitrate (NO_3^-), and phosphate (PO_4^{3-}), Chemosphere 119 (2015) 646–653.
[8] S. Uludag-Demirer, M. Othman, Removal of ammonium and phosphate from the supernatant of anaerobically digested waste activated sludge by chemical precipitation, Bioresour. Technol. 100 (2009) 3236–3244.
[9] M. Andalib, G. Nakhla, J. Zhu, High rate biological nutrient removal from high strength wastewater using anaerobic-circulating fluidized bed bioreactor (A-CFBBR), Bioresour. Technol. 118 (2012) 526–535.
[10] Z. Ma, Q. Li, Q. Yue, B. Gao, W. Li, X. Xu, Q. Zhong, Adsorption removal of ammonium and phosphate from water by fertilizer controlled release agent prepared from wheat straw, Chem. Eng. J. 171 (2011) 1209–1217.
[11] J. Choi, J. Ryu, K. Kwon, M. Song, S. Lee, S. Kim, S. Lee, Adsorption of ammonium nitrogen and phosphate onto basanite and evaluation of toxicity, Water Air Soil Pollut. 225 (2014) 2059–2070.
[12] L.F. Greenlee, D.F. Lawler, B.D. Freeman, B. Marrot, P. Moulin, Reverse osmosis desalination: Water sources, technology, and today's challenges, Water Res. 43 (2009) 2317–2348.
[13] C. Li, Y. Dong, Y. Lei, D. Wu, P. Xu, Removal of low concentration nutrients in hydroponic wetlands integrated with zeolite and calcium silicate hydrate functional substrates, Ecol. Eng. 82 (2015) 442–450.
[14] W. Huang, R. Zhu, F. He, D. Li, Y. Zhu, Y. Zhang, Enhanced phosphate removal from aqueous solution by ferric-modified laterites: Equilibrium, kinetics and thermodynamic studies, Chem. Eng. J. 228 (2013) 679–687.

[15] W. Huang, D. Li, Z. Liu, Q. Tao, Y. Zhu, J. Yang, Y. Zhang, Kinetics, isotherm, thermodynamic, and adsorption mechanism studies of $La(OH)_3$-modified exfoliated vermiculites as highly efficient phosphate adsorbents, Chem. Eng. J. 236 (2014) 191–201.
[16] W. Huang, J. Chen, F. He, J. Tang, D. Li, Y. Zhu, Y. Zhang, Effective phosphate adsorption by Zr/Al-pillared montmorillonite: insight into equilibrium, kinetics and thermodynamics, Appl. Clay Sci. 104 (2015) 252–260.
[17] Y.R. Wang, D.C. Tsang, W.E. Olds, P.A. Weber, Utilizing acid mine drainage sludge and coal fly ash for phosphate removal from dairy wastewater, Environ. Technol. 34 (2013) 3177–3182.
[18] S. Wei, W. Tan, F. Liu, W. Zhao, L. Weng, Surface properties and phosphate adsorption of binary systems containing goethite and kaolinite, Geoderma 213 (2014) 478–484.
[19] W. Huang, X. Yu, J. Tang, Y. Zhu, Y. Zhang, D. Li, Enhanced adsorption of phosphate by flower-like mesoporous silica spheres loaded with lanthanum, Microporous Mesoporous Mater. 217 (2015) 225–232.
[20] X. Ji, M. Zhang, Y. Wang, Y. Song, Y. Ke, Y. Wang, Immobilization of ammonium and phosphate in aqueous solution by zeolites synthesized from fly ashes with different compositions, J. Ind. Eng. Chem. 22 (2015) 1–7.
[21] E.B. Simsek, E. Özdemir, U. Beker, Zeolite supported mono- and bimetallic oxides: Promising adsorbents for removal of As(V) in aqueous solutions, Chem. Eng. J. 220 (2013) 402–411.
[22] A. Alshameri, A. Ibrahim, A.M. Assabri, X. Lei, H. Wang, C. Yan, The investigation into the ammonium removal performance of Yemeni natural zeolite: Modification, ion exchange mechanism, and thermodynamics, Powder Technol. 258 (2014) 20–31.
[23] D. Guaya, C. Valderrama, A. Farran, C. Armijos, J.L. Cortina, Simultaneous phosphate and ammonium removal from aqueous solution by a hydrated aluminum oxide modified natural zeolite, Chem. Eng. J. 271 (2015) 204–213.
[24] L. Zhang, Q. Zhou, J. Liu, N. Chang, L. Wan, J. Chen, Phosphate adsorption on lanthanum hydroxide-doped activated carbon fiber, Chem. Eng. J. 185–186 (2012) 160–167.
[25] J. Tang, J. Chen, W. Huang, D. Li, Y. Zhu, Y. Tong, Y. Zhang, Porous $Pr(OH)_3$ nanowires as novel high-performance adsorbents for phosphate removal, Chem. Eng. J. 252 (2014) 202–209.
[26] A. Ghosh, S. Chakrabarti, U.C. Ghosh, Fixed-bed column performance of Mn-incorporated iron(III) oxide nanoparticle agglomerates on As(III) removal from the spiked groundwater in lab bench scale, Chem. Eng. J. 248 (2014) 18–26.
[27] T.A.H. Nguyen, H.H. Ngo, W.S. Guo, T.Q. Pham, F.M. Li, T.V. Nguyen, X.T. Bui, Adsorption of phosphate from aqueous solutions and sewage using zirconium loaded okara (ZLO): Fixed-bed column study, Sci. Total Environ. 523 (2015) 40–49.
[28] M.R. Awual, A. Jyo, Assessing of phosphorus removal by polymeric anion exchangers, Desalination 281 (2011) 111–117.
[29] M. Jain, V.K. Garg, K. Kadirvelu, Cadmium(II) sorption and desorption in a fixed bed column using sunflower waste carbon calcium–alginate beads, Bioresour. Technol. 129 (2013) 242–248.
[30] E.I. Unuabonah, M.I. El-Khaiary, B.I. Olu-Owolabi, K.O. Adebowale, Predicting the dynamics and performance of a polymer-clay based composite in a fixed bed system for the removal of lead (II) ion, Chem. Eng. Res. Des. 90 (2012) 1105–1115.
[31] X. Sun, T. Imai, M. Sekine, T. Higuchi, K. Yamamoto, A. Kanno, S. Nakazono, Adsorption of phosphate using calcined Mg_3–Fe layered double hydroxides in a fixed-bed column study, J. Ind. Eng. Chem. 20 (2014) 3623–3630.
[32] C.A. Demarchi, A. Debrassi, J.D. Magro, N. Nedelko, A. Ślawska-Waniewska, P. Dłużewski, J. Greneche, C.A. Rodrigues, Adsorption of Cr(VI) on crosslinked chitosan-Fe(III) complex in fixed-bed systems, J. Water Process Eng. 7 (2015) 141–152.
[33] E.D. Woumfo, J.M. Siéwé, D. Njopwouo, A fixed-bed column for phosphate removal from aqueous solutions using an andosol-bagasse mixture, J. Environ. Manage. 151 (2015) 450–460.
[34] S.S. Baral, N. Das, T.S. Ramulu, S.K. Sahoo, S.N. Das, G.R. Chaudhury, Removal of Cr(VI) by thermally activated weed Salvinia cucullata in a fixed-bed column, J. Hazard. Mater. 161 (2009) 1427–1435.
[35] W.W.J.L. Ling Zhang, X. Wang, Removal of phosphate from water using raw and activated laterite: Batch and column studies, Desalin. Water Treat. 52 (2014) 775–783.
[36] V.J.I.M.M.A. Stylianou, Comparison of Mn, Zn, and Cr removal in fluidized- and fixed-bed reactors by using clinoptilolite, Desalin. Water Treat. 53 (2015) 3355–3362.
[37] A.A.H.A. Solmaz Saadat, Mathematical modeling of the Ni(II) removal from aqueous solutions onto pretreated rice husk in fixed-bed columns: A comparison, Desalin. Water Treat. (2015) 1–12.
[38] P.A. Kumar, S. Chakraborty, Fixed-bed column study for hexavalent chromium removal and recovery by short-chain polyaniline synthesized on jute fiber, J. Hazard. Mater. 162 (2009) 1086–1098.
[39] A. Ghosh, S. Chakrabarti, U.C. Ghosh, Fixed-bed column performance of Mn-incorporated iron(III) oxide nanoparticle agglomerates on As(III) removal from the spiked groundwater in lab bench scale, Chem. Eng. J. 248 (2014) 18–26.
[40] E.W. Shin, K.G. Karthikeyan, M.A. Tshabalala, Orthophosphate sorption onto lanthanum-treated lignocellulosic sorbents, Environ. Sci. Technol. 39 (2005) 6273–6279.
[41] H. Li, J. Ru, W. Yin, X. Liu, J. Wang, W. Zhang, Removal of phosphate from polluted water by lanthanum doped vesuvianite, J. Hazard. Mater. 168 (2009) 326–330.
[42] J. Liu, Q. Zhou, J. Chen, L. Zhang, N. Chang, Phosphate adsorption on hydroxyl–iron–lanthanum doped activated carbon fiber, Chem. Eng. J. 215–216 (2013) 859–867.